Bioinformatics, 2024, pp. 1–9

doi: DOI HERE
Advance Access Publication Date: Day Month Year
Paper

PAPER

Bayesian Modeling of Time Series Data (BayModTS) - A FAIR Workflow to Process Sparse and Highly Variable Data

Sebastian Höpfl,[1] Mohamed Albadry,[2,3] Uta Dahmen,[2] Karl-Heinz Herrmann,[4] Eva Marie Kindler,[6] Matthias König,[5] Jürgen Rainer Reichenbach,[4] Hans-Michael Tautenhahn,[7] Weiwei Wei,[2] Wan-Ting Zhao[4] and Nicole Erika Radde[1,*]

[1]Institute for Stochastics and Applications, University of Stuttgart, Pfaffenwaldring 9, 70596, Stuttgart, Germany, [2]Experimental Transplantation Surgery, Department of General, Vascular and Visceral Surgery, University Hospital Jena, Drackendorferstr. 1, 07745, Jena, Germany, [3]Department of Pathology, Faculty of Veterinary Medicine, Menoufia University, Shebin Elkom, Menoufia, Egypt, [5]Institute for Biology, Faculty of Life Sciences, Humboldt-University Berlin, Philippstraße 13, 10115, Berlin, Germany, [4]Medical Physics Group, Institute for Diagnostic and Interventional Radiology, University Hospital Jena, Philosophenweg 3, 07743, Jena, Germany, [6]Clinic for General- Visceral- and Vascular Surgery, Jena University Hospital, Am Klinikum 1, 07747, Jena, Germany and [7]Clinic for Visceral, Transplantation, Thoracic and Vascular Surgery, Leipzig University Hospital, Liebigstrasse 20, 04103, Leipzig, Germany
[*]Corresponding author. nicole.radde@simtech.uni-stuttgart.de
FOR PUBLISHER ONLY Received on Date Month Year; revised on Date Month Year; accepted on Date Month Year

Abstract

Motivation. Systems biology aims to better understand living systems through mathematical modelling of experimental and clinical data. A pervasive challenge in quantitative dynamical modelling is the integration of time series measurements, which often have high variability and low sampling resolution. Approaches are required to utilise such information while consistently handling uncertainties.

Results. We present BayModTS (Bayesian Modeling of Time Series data), a new FAIR (Findable, Accessible, Interoperable and Reusable) workflow for processing and analysing sparse and highly variable time series data. BayModTS consistently transfers uncertainties from data to model predictions, including process knowledge via parameterised models. Further, credible differences in the dynamics of different conditions can be identified by filtering noise. To demonstrate the power and versatility of BayModTS, we applied it to three hepatic datasets gathered from three different species and with different measurement techniques: (i) blood perfusion measurements by magnetic resonance imaging in rat livers after portal vein ligation, (ii) CT-based volumetric assessment of human liver remnants after clinical liver resection, and (iii) pharmacokinetic time series of different drugs in normal and steatotic mice.

Availability and Implementation. The BayModTS codebase is available on GitHub at `https://github.com/Systems-Theory-in-Systems-Biology/BayModTS`. The repository contains a Python script for the executable BayModTS workflow and a widely applicable SBML (Systems Biology Markup Language) model for retarded transient functions. In addition, all examples from the paper are included in the repository. Data and code of the application examples are stored on DaRUS `https://doi.org/10.18419/darus-3876` - private link for review: `https://darus.uni-stuttgart.de/privateurl.xhtml?token=fbf32426-5164-4455-85bf-8c9604ea44fc`. The raw data of the MRI ROI voxel data were uploaded to DaRUS `https://doi.org/10.18419/darus-3878` - private link for review: `https://darus.uni-stuttgart.de/privateurl.xhtml?token=b5e04561-26b3-4261-9bdc-b55b687363a0`. The steatosis metabolite data are published on FairdomHub `10.15490/fairdomhub.1.study.1070.1`.

Contact. nicole.radde@simtech.uni-stuttgart.de

Key words: Time Series Data, Bayesian Inference, Posterior Predictive Distribution, SBML, FAIR Principles, Hepatology

Key Messages

- BayModTS is a FAIR workflow that uses parameterised models to process sparse and highly variable time series data
- BayModTS transforms measurements into time-continuous functions equipped with credibility bounds
- BayModTS is broadly applicable, as demonstrated using three different datasets collected in a hepatological context, and can be used to credibly discriminate conditions.

Introduction

Biology is a field of extremes with extensive high-throughput data (e.g. omics data) on the one hand and sparse data (e.g. western blots) on the other. These data are generally characterised by high variability caused by inherent biological variation and measurement uncertainties. Due to cost and ethical aspects, small sample sizes further complicate the calculation of reliable statistics. In such a setting, it is essential to use the acquired data to make progress in the field and steer biological and medical research in promising directions.

A recurring challenge in biomedical data analysis is comparing the temporal response under two different conditions, i.e., comparing two time series. The current standards in biology for investigating differences in time series data are pairwise hypothesis tests, testing each time point separately (Huang *et al.*, 2022; Ko *et al.*, 2023; Wei *et al.*, 2022) or comparison of derived parameters such as the area under the curve, e.g. in pharmacokinetics (Scheff *et al.*, 2011; Chen *et al.*, 2022; Hughes *et al.*, 2019). Both methods are frequency-oriented and have the problem of extensive multiple testing if each time point is used as a single sample. Moreover, information about the dynamics is lost when using a summary statistic such as the area under the curve. Methods that take the dynamics of the data into account are, e.g., Semi Metric Ensemble Time Series (SMETS) (Tapinos and Mendes, 2013) and the use of confidence bands (Korpela *et al.*, 2014). SMETS can compare multivariate time series by measuring their pairwise distance, and frequentistic confidence bands of different datasets can be compared to each other.

Another challenge with sparse and noisy time series data is dealing with outliers, which can drastically distort the results. As defined by Hawkings, an outlier is an observation that deviates so strongly from other observations that it is suspected of being caused by a different mechanism (Hawkins, 1980). However, the question of suspicion is not easy to answer if only a few replicates are available. Existing methods for detecting single point outliers are the z-score, the Grubbs-Test (Grubbs, 1950), the Tietjen-Moore test (Tietjen and Moore, 1972), and Dixon's Q test (Rorabacher, 1991). Further, time series filtering (e.g. bandpass filters) and dynamic linear models (Campagnoli *et al.*, 2009) can smooth data series and identify outliers by taking the dynamics into account. Here, we argue against outlier classification in sparse data settings without incorporating process knowledge. The potential pitfall is a substantial information loss by excluding outliers in sparse data settings. Using Bayesian inference with all available data, outliers are inherently corrected by incorporating process knowledge.

Fortunately, time series data are an example where knowledge of the underlying dynamics is often available. Here, we present BayModTS (Bayesian Modeling of Time Series data), a novel Findable, Accessible, Interoperable and Reusable (FAIR) workflow for processing time series data that incorporates process knowledge. BayModTS is designed for sparse data with low temporal resolution, a small number of replicates and high variability between replicates. BayModTS is based on a simulation model of the temporal behaviour of the underlying data generation process. This simulation model can be an Ordinary Differential Equation (ODE), a time-parameterized function, or any other dynamic modelling approach. For model calibration, posterior distributions of the parameters are sampled using a Bayesian approach. Ensembles of these posterior distributions are then used for forward simulations that can be compared to the data. This framework allows us to investigate whether conditions are credibly different, using measures from statistics and information theory such as credibility intervals. Importantly, BayModTS is based on systems biology modelling standards and is easily understandable and accessible for experts and novices.

We demonstrate the broad applicability of BayModTS using three data sets that investigate different characteristics of the liver in animals and human patients. These data were collected using fundamentally different measurement methods: (i) quantification of blood perfusion changes in the liver lobes of rats after Portal Vein Ligation (PVL) using Magnetic Resonance Imaging (MRI), (ii) Computer Tomography (CT)-based volumetric assessment of the liver remnant in human patients after clinical liver resections, and (iii) quantification of metabolic drug concentrations in mice via ultra-performance liquid chromatography-tandem mass spectrometry (UPLC-MS/MS). BayModTS enables to generate hypotheses about differences in conditions in these application scenarios. In particular, BayModTS deals with intra- and inter-individual variation in the studies by focusing on condition differences rather than population heterogeneity. The results are discussed in their respective biological and medical contexts.

The BayModTS workflow

Inputs to BayModTS are (i) serial data $D = \{m^{(j)}(t_k)\}$, with time points $k = 1, \ldots, T$ that do not have to be equidistant, and $j = 1, \ldots, N$ replicates per time point, (ii) an associated simulation model $s(t, \theta)$ with parameters θ, and (iii) a prior distribution $p(\theta)$ on the model parameters (Fig. 1).

The model can be defined in SBML (Keating *et al.*, 2020) and is part of the PEtab (Schmiester *et al.*, 2021) format. BayModTS uses Retarded Transient Dynamics (RTD) functions (Kreutz, 2020)

$$f_{TF}(t) = \underbrace{A_{\text{sus}}\left(1 - e^{-\frac{t}{t_1}}\right)}_{\text{sustained response}} + \underbrace{A_{\text{trans}}\left(1 - e^{-\frac{t}{t_{11}}}\right)e^{-\frac{t}{t_2}}}_{\text{transient response}} + p_0 \quad (1)$$

with transformed time

$$t = \log_{10}\left(10^{t_{\text{real}} \cdot \frac{10}{T_{\text{range}}}} + 10^{T_{\text{shift}}}\right) - \log_{10}\left(1 + 10^{T_{\text{shift}}}\right) \quad (2)$$

as a universal simulation model $s(t, \theta)$ with parameters

$$\theta = (A_{\text{sus}}, t_1, A_{\text{trans}}, t_{11}, t_2, T_{\text{shift}}, T_{\text{range}}, p_0). \quad (3)$$

Equ. (1) consists of a transient and a persistent activation term. RTD functions can describe the responses of many biological processes to various inputs without knowing the system's detailed interactions a priori. RTD responses can be delayed by a shift parameter T_{shift} via a non-linear time transformation that leaves $t = 0$ invariant (Equ. (2)). An immediate response corresponds to $T_{\text{shift}} = -2$ (Kreutz, 2020). The parameter T_{range} scales time to the observation interval. Even if the system under investigation can be described by an ODE model, RTD functions can serve as computationally advantageous surrogate models because they can be evaluated directly without numerical integration.

PEtab is a reproducible format for a parameter estimation problem. It contains information about the estimated

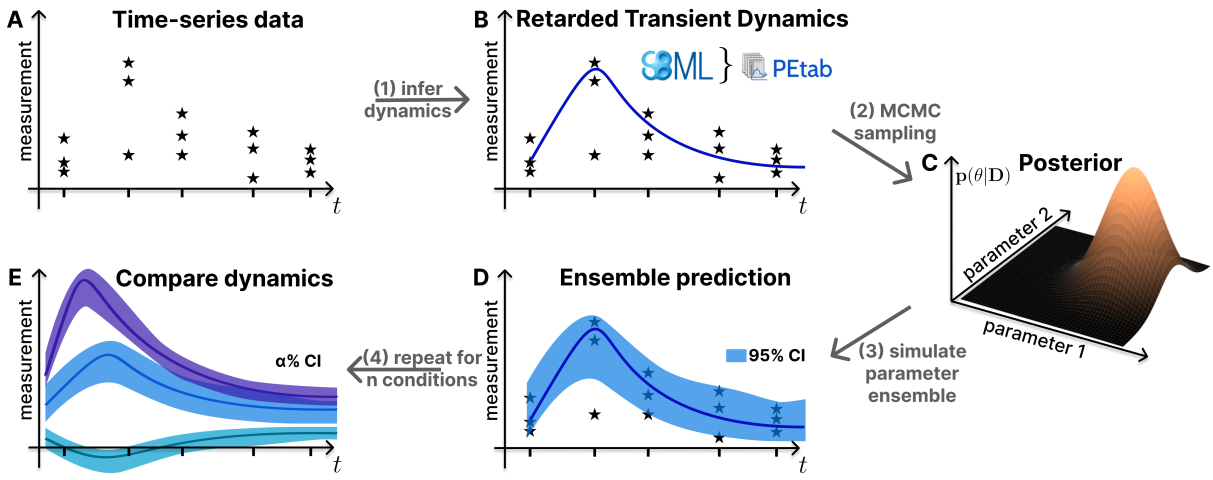

Fig. 1. The FAIR BayModTS workflow reveals credible regions in the data space. BayModTS applies a statistical Bayesian framework and a simulation model $s(t, \theta)$ to transform sparse and highly variable time series data into less noisy time courses with uncertainty estimates for model states. A. Time series data and B. RTD functions as a universal simulation model $s(t, \theta)$ are used as input together with parameter priors. C. The Posterior distribution $p(\theta|D)$ is inferred using MCMC sampling. D. Simulated parameter posterior sample trajectories (Ensembles) are used to infer summary statistics that quantify model state uncertainties. We use 95% CI tubes. E. Dynamics under different conditions can be compared via CI tubes.

parameters θ, the experimental conditions, the observed data D and the error model needed to define the likelihood function $L_D(\theta)$. Here, we assume additive, independent, and identically distributed (i.i.d.) Gaussian measurement errors with equal variances σ^2 for all measurements,

$$m(t_k) = s(t_k, \theta) + \epsilon \quad \epsilon \sim \mathcal{N}(0, \sigma^2), \tag{4}$$

leading to

$$L_D(\theta) = \prod_{k=1}^{T} \prod_{j=1}^{N} \frac{1}{\sqrt{2\pi}\sigma} \exp\left(-\frac{\left(s(t_k, \theta) - m^{(j)}(t_k)\right)^2}{2\sigma^2} \right). \tag{5}$$

The variance σ^2 can be treated as an additional unknown parameter that has to be estimated in the inverse problem or set to a fixed value for each data point or measurement series. Different approaches exist for formulating an appropriate error model and choosing hyperparameters for this model (Kreutz *et al.*, 2007; Thomaseth and Radde, 2023). Our pragmatic approach pools all data for estimating σ, assuming that the noise is mainly determined by the measurement method and does not vary much between time points. PEtab can be used for maximum likelihood estimation or sampling-based approaches. Here, we infer parameters from the posterior distribution (Fig. 1C)

$$p(\theta|D) \propto p(D|\theta) \cdot p(\theta) \tag{6}$$

in a statistical Bayesian setting to quantify the uncertainty in the parameter space. Inference is based on Markov Chain Monte Carlo (MCMC) sampling techniques to generate posterior samples $\theta^{(i)}$, $i = 1, \ldots, P$ (Fig. 1 step (2)). For RTD functions, uniform priors with wide bounds around the measurement data can be used (Kreutz, 2020) and adapted for other scenarios.

Posterior predictive distributions (PPDs)

$$p(\tilde{D}|D) = \int p(\tilde{D}, \theta|D) d\theta \tag{7}$$

propagate the uncertainty from the parameter into the data space. Using factorization of the joint density $p(\tilde{D}, \theta|D)$ and exploiting that the PPD of any dataset $\tilde{D}$ is independent of D given the model parameters, we can reformulate (7),

$$p(\tilde{D}|D) = \int p(\tilde{D}|\theta, D) p(\theta|D) d\theta \tag{8a}$$

$$= \int p(\tilde{D}|\theta) p(\theta|D) d\theta. \tag{8b}$$

Using the posterior samples $\theta^{(i)}$, these PPDs can be estimated via Monte Carlo integration,

$$p(\tilde{D}|D) \approx \frac{1}{P} \sum_{i=1}^{P} p(\tilde{D}|\theta^{(i)}). \tag{9}$$

A lower bound for the variability of the PPD can be obtained by using summary statistics of simulation model trajectories $s(t, \theta)$ evaluated with posterior samples $\theta^{(i)}$,

$$s^{(i)}(t) = s(t, \theta^{(i)}), \tag{10}$$

without adding measurement noise. Summary statistics derived from these sample trajectories represent the remaining uncertainties of the model states $s(t, \theta)$. In BayModTS, (1-α)·100% Credibility Interval (CI) tubes of the model states are used to quantify the uncertainty. CIs are obtained for each time point by calculation of the percentile ranges $[z_{\frac{\alpha}{2}}, z_{1-\frac{\alpha}{2}}]$ from all sample trajectories $s^{(i)}(t)$ (Fig. 1 step (3)). For visualisation, the point-wise CIs are linearly interpolated and can be interpreted as model-informed noise filters. Data points far outside those tubes might be seen as suspicious points that need further investigation or can be classified as outliers based on the model assumption. The procedure can be repeated if the data set includes time courses from multiple conditions. CI tubes can be used to compare dynamics under different conditions (Fig. 1 step (4) and Fig. 1E).

Regarding FAIR principles, BayModTS is interoperable and reusable using the PEtab format, which contains all information about the inference problem. Findability and accessibility are ensured by uploading the analysis results to an open public repository and assigning a Digital Object Identifier (DOI). We provide a PEtab file containing the RTD function SBML model and executable code for the Bayesian analysis on GitHub (https://github.com/Systems-Theory-in-Systems-Biology/BayModTS). Both can be easily adapted for either more complex models, different conditions, and individual data. The posterior is sampled via algorithms of the PyPesto toolbox (Schälte *et al.*, 2021). PyPesto is well received and maintained by the systems biology model community and includes, besides others, an adaptive Metropolis-Hastings algorithm, a parallel tempering algorithm, and a wrapper to the ensemble sampler emcee (Foreman-Mackey *et al.*, 2013). We recommend examining the sampling convergence via measures such as the Effective Sample Size (ESS), visually via traces, or via the Gelman–Rubin diagnostic for multiple chains.

Application Examples

Biological context: Hepatocellular carcinoma (HCC) is among the leading causes of cancer-related deaths worldwide and has the fastest-growing number of cancer-related deaths in the United States (El-Serag and Rudolph, 2007). Still, Africa and Asia are showing the highest incidences of HCC as Hepatitis B and C are most prevalent in these continents and the leading cause of chronic liver diseases and HCC (Ferlay *et al.*, 2015). Based on evidence, liver resection is the most promising treatment option for HCC, but randomised phase III trials are ongoing (Vogel *et al.*, 2018; Elderkin *et al.*, 2023). However, liver resections are complex and pose the risk of major complications (Abreu *et al.*, 2020). Portal Vein Embolization (PVE), the clinical pendant to PVL in animal models, is often performed to induce growth of the future liver remnant. In PVE, the portal influx of diseased liver lobes is ligated, leading to hypoperfusion and undersupply of nutrients in these lobes. In contrast, the non-ligated lobes are hyperperfused, inducing regeneration and hypertrophy. However, the relationship between the gain in liver mass of the non-ligated liver lobes and liver function is still poorly understood (Christ *et al.*, 2021). Moreover, comorbidities such as a high degree of hepatic steatosis might impair the proper functioning and recovery of the remaining liver volume after resection (Veteläinen *et al.*, 2007).

Quantification of blood perfusion changes in the liver lobes of rats after PVL

This study explored in vivo liver perfusion in rats' ligated and non-ligated liver lobes. In total, 25 rats were subjected to 60% PVL. The experimental procedure involved ligation of the left stem of the portal vein supplying the Left Median (LML) and Left Lateral Lobe (LLL) and the right stem supplying the Right Lobe (RL) (Fig. 2A). As a result, the remaining non-ligated Caudate Lobe (CL) and Right Median Lobe (RML) of the liver were hyperperfused.

Changes in local tissue perfusion over time were monitored and quantified using MRI in a cross-sectional study design. Perfusion was quantitatively assessed at the voxel level using arterial spin labelling (ASL) (Jahng *et al.*, 2014), which is based on labelling spins of arterial blood by pulsed inversion and subtraction of the resulting image from a control image acquired without labelling. Negative values resulting from this subtraction were excluded as they have no physiological relevance.

Perfusion was assessed using manually defined Regions of Interest (ROIs) in the different liver lobes. In this case, the ROIs are representative of the perfusion of the lobes. The ROI selection is shown as an example for the RML (Fig. 2B). The increased perfusion observed on postoperative day one (POD1) in the RML (Fig. 2B second picture) is visually recognisable by the increasing yellow to red colouration in the annotated region. Individual voxel-level perfusion values within each lobe ROI for the entire dataset (i.e., all 25 animals) are shown in Fig. 2C for the different time points. The observed variability in individual voxel values is large due to blood flow and pulsation in larger vessels. Further reasons for the high variability are that different ROIs differ in the number and size of vessels they contain and the biological variation between animals. This variability makes it difficult to identify a consistent trend over time by visually inspecting these raw data.

Following the current standard processing of MRI ROI data and averaging the individual voxel data per liver lobe in the animals, the result of this averaging can be visualised as box plots with reduced variability (Fig. 2D). Inspection of the averaged data shows that the unligated lobes (i.e., RML and CL) were transiently hyperperfused on POD1 and POD2, whereas perfusion in the ligated lobes decreased after POD1.

On the other hand, BayModTS processing of the individual voxel data results in time-continuous and smooth CI tubes (Fig. 2E), considerably reduces the variability, and reveals that the highest uncertainty is between POD0 and POD1. The CI tubes provide a credible and clear visual distinction between the dynamics of the hyper- and the hypoperfused lobes. For all three ligated lobes (LML, LLL, RL), the average perfusion values decrease by about 30-50% within one day and remain at low values. At the same time, the non-ligated lobes (RML, CL) are hyperperfused, which is most pronounced at POD1. The median perfusion of CL is already back to pre-PVL levels by POD2, which occurs more slowly in the RML.

The LML showed the greatest variability in perfusion compared to the other liver lobes. Reasons for the uncertainty are the proximity of the LML to the heart, which caused motion that affected the measurements, and the putative development of collaterals leading to portal inflow of unknown degree. In addition, the heart, liver and lung tissues are not equally susceptible to the magnetic field, causing B0 inhomogeneities that distort the MRI images. As a result, slice positions close to the lungs and heart, such as the LML, usually have poor image quality. Consequently, cardiac motion and B0 inhomogeneities reduce the usable ROI size and thereby increase the uncertainty, which is also reflected in the size of the CI tubes. Consistent with this, the 95% CI of the noise parameter σ (Fig. 2F) is also the largest for LML, reflecting higher measurement noise. Overall, all noise parameters were well-identifiable.

Conditions can also be compared by looking at the marginal posterior distributions of the model parameters. This is exemplified by the marginal posterior distributions of the parameter p_0, which describes the preoperative perfusion in each of the lobes (Fig. 2G). Here again, the LML p_0 CI is the largest, consistent with an overall increased uncertainty of the CI tubes. The preoperative perfusion of the RL is credibly lower than that of all other lobes (the upper limit of the RL CI is below the lower limit of all other CIs). Here, the relatively low RL perfusion is likely an artefact of having fewer vessels

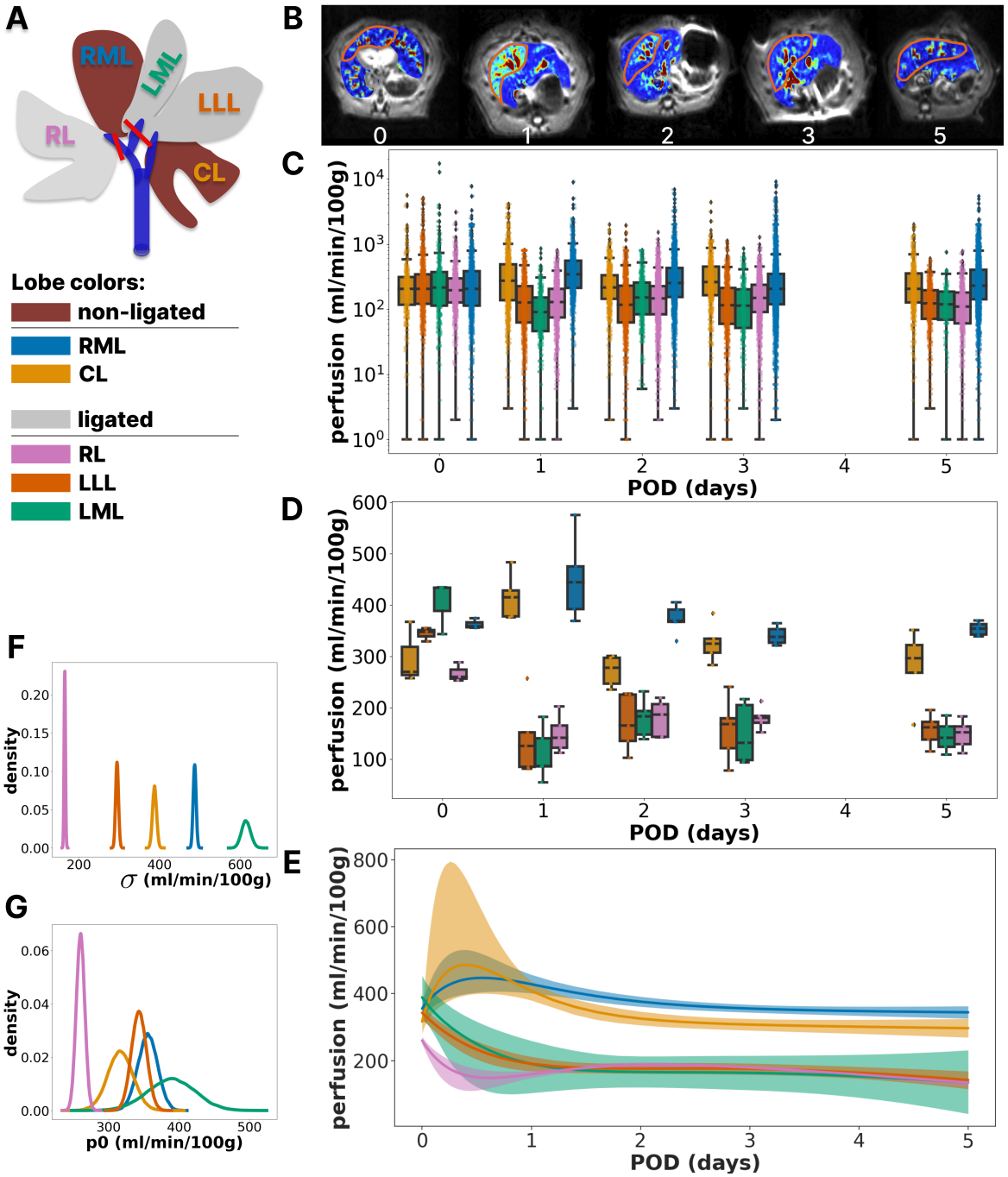

Fig. 2. BayModTS analysis to extract perfusion courses in ligated and non-ligated liver lobes from MRI data after PVL. A. Illustration of ligated (hypoperfused) and non-ligated (hyperperfused) lobes of a rat liver subjected to PVL. B. Exemplary MRI images for 0, 1, 2, 3 and 5 Post Operative Days (POD). The area outlined in orange refers to the Region Of Interest (ROI) annotation for RML. Perfusion is colour-coded, with yellow to red values indicating high values. C. Boxplots of individual voxel values in the selected ROIs of $n = 5$ animals per time point (raw data). D. State-of-the-art visualisation of MRI ROI data. Boxplots are based on per-animal averaged ROI voxel data. E. BayModTS ensemble perfusion predictions with median (solid lines) and 95% CI tubes for all lobes. F, G. Marginal distributions of the parameters σ and p_0 per lobe, restricted to the 95% highest density interval.

in the typical RL slice, which disappears in the postoperative measurements.

In conclusion, BayModTS provided a continuous and credible prediction of postoperative liver perfusion in the different lobes after PVL. The credibility bounds allowed us to hypothesise, for example, the timing of hyperperfusion and the time scales of adaptation. Furthermore, the continuity of the BayModTS results allows the PVL data to be used as input for physiological models. In the future, this information could provide valuable information for determining the correct timing of surgery in human patients without the need for repeated MRI scans.

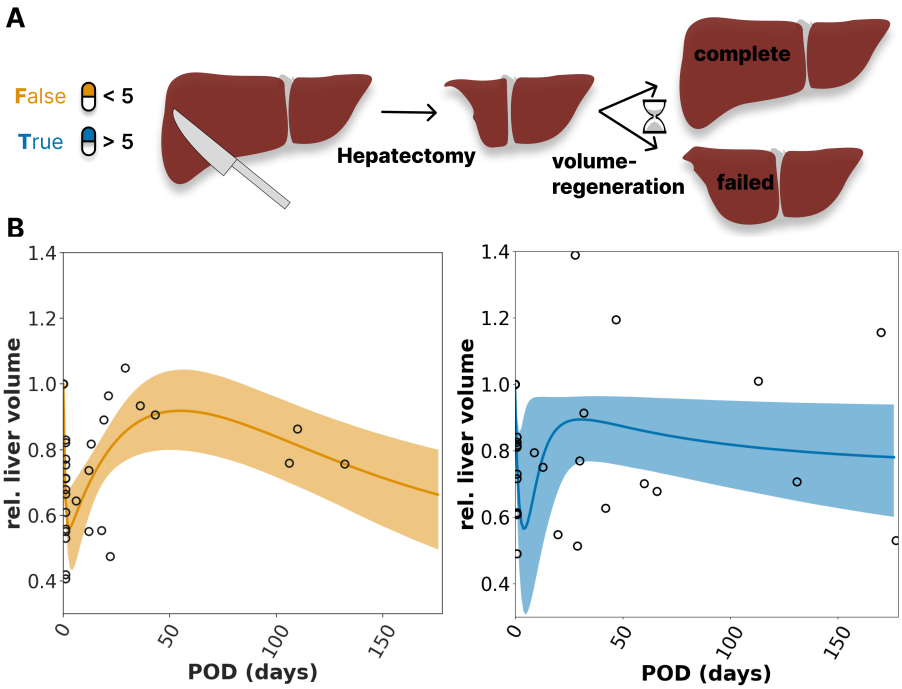

Fig. 3. BayModTS analysis applied to postoperative liver volumes of patients subject to extended liver resection. Comparison of non-polypharmaceutic (orange) and polypharmaceutic (blue) regeneration courses after liver resection. A. Volume regeneration of human livers was monitored pre- and post-hepatectomy. B, Non-polypharmaceutic (left) and polypharmaceutic (right) liver regeneration data (o) along with inferred median (dark lines) and 95% CI tubes (shaded areas).

Postoperative liver regeneration after resection

In humans, benign and malignant liver lesions may require extensive partial resection of the liver. Clinical CT-based liver volumetry studies can assess postoperative liver regeneration after resection. In most cases, the liver regenerates and regains its original volume within a few weeks after resection (Fig. 3A). However, various factors, such as the extent of the resection, pre-existing liver cell damage, previous illnesses, or postoperative complications, influence the course of regeneration after the operation. Given the increasing number of elderly patients requiring such a resection (Reddy *et al.*, 2011), the superordinate ZeLeR-study (ethical vote: 2018-1246-Material) aims to investigate the influence of age and secondary confounding variables such as polypharmacy (= more than five medications per day). Postoperative volume regeneration of the liver was investigated in 21 patients from two different age groups (<46 years and >64 years). All patients underwent extended partial liver resection at Jena University Hospital between 03/2019 and 10/2022 as part of the study. In addition to age, influencing factors such as polypharmacy, multimorbidity, gender and extent of resection were recorded. The patients underwent preoperative imaging, usually CT (computed tomography) and, less frequently, MRI. All images obtained within 6 months postoperatively were used to assess postoperative volume recovery. Liver volumes were determined using the Synapse3D software (Fujifilm).

The data are shown in Fig. 3B. Here, we focus on the distinction between non-polypharmaceutical patients (False) and polypharmaceutical patients (True). The data are normalised to preoperative liver volume to account for differences in baseline liver volumes. It is noted that data points at later times likely correspond to liver volumes of patients with complications in the postoperative course and, therefore, remained under observation. Patients without complications dropped out of the study within a few days after resection. Furthermore, in some cases the liver volume increases rapidly after hepatectomy and temporarily exceeds the original volume, leading to values above 1. A mechanistic model that mimics the underlying data generation process should account for all these peculiarities. In addition, the courses are further distorted by patient differences. Due to these facts, no clear trend could be identified in the data.

We use BayModTS with RTD functions as a flexible phenomenological model to describe the data. Our approach captures the data of non-polypharmaceutical patients (orange curve) well (Fig. 3B left). The volume courses increase within a few weeks after resection but drop considerably afterwards. As explained before, this drop is probably an artefact of screening only patients with complications at that time. The data of polypharmaceutical patients has greater variability, which is not as well captured by the BayModTS CI tubes (Fig. 3B right). In contrast to the non-polypharmaceutical patients, the decrease in volume on the longer time scale is less pronounced. Overall, interpreting these results and comparing the two groups is difficult due to the small sample size and the many confounding factors that would require a multi-factorial analysis.

In summary, BayModTS improved the visualisation of this heterogeneous liver volume dataset from hepatectomy patients. We plan to extend this analysis as more data becomes available. Particularly in patients with pre-existing diseases, knowledge of the progression of liver regeneration could improve the planning and execution of resections.

Influence of steatosis on drug metabolization dynamics in mice

Hepatic steatosis is a common liver disease affecting up to 25% of the population in the Western world (Younossi *et al.*, 2023). However, the effects of hepatic steatosis on drug metabolism remain poorly understood.

The study by Albadry *et al.* (2022) aimed to investigate the influence of different degrees of hepatic steatosis on the pharmacokinetics of several test drugs. Mice were fed a high-fat methionine-choline deficient (MCD) diet for two or four weeks, resulting in micro- and macrosteatosis (Fig. 4A). A drug cocktail consisting of codeine, caffeine and midazolam was administered and whole blood samples were analysed to determine drug concentrations. Peak concentrations for all three test drugs occurred within 15-60 minutes, followed by elimination of the drug within 4-6 hours. The time course measurements showed high inter-individual variability (Fig. 4B), with time-varying variances within a condition, which made it difficult to compare conditions over the entire period.

We used BayModTS to assess the elimination dynamics of all substrates as a function of steatosis degree. In the original study (Albadry *et al.*, 2022), this was accomplished by assuming an exponential decay kinetics that mimics drug degradation.

Results of the BayModTS analysis with the RTD model are depicted in Fig. 4C. BayModTS reduced the uncertainty in the data markedly for all time courses. Our analysis suggests that macrovesicular periportal steatosis (4 weeks) delayed the clearance of all test drugs. Moreover, peak concentrations of caffeine and midazolam were higher in macrovesicular steatosis.

In summary, BayModTS helped to understand the data regarding differences in pharmacokinetics and indicated an impaired metabolisation in mice with macrosteatosis.

Discussion

We have introduced BayModTS, a novel workflow for processing time series data using a FAIR Bayesian analysis. BayModTS can be applied in scenarios with sparse and noisy data. The robustness is based on a simulation model that can mimic the measured time series. The statistical Bayesian framework enables a consistent transfer of data variability to uncertainties in model parameters, thereby acting as a noise filter and reducing the impact of potential outliers. BayModTS can process data in areas where purely data-driven approaches fail. The BayModTS-derived dynamics can be used to compare conditions or as continuous-time input equipped with uncertainty for computational models. Our examples show broad applicability in different contexts and for different kinds of data. Various settings, such as choices of priors or simulation and error models, can be flexibly adapted to specific use cases. Importantly, BayModTS contributes to reproducibility according to the FAIR principles by using established tools in the systems biology community and adhering to standard reporting guidelines (Tiwari *et al.*, 2021; Kruschke, 2021).

Properly describing observed data distributions in connection with deterministic simulation models is tricky in Bayesian settings. Forward simulations with posterior samples can filter noise because the model assumption restricts the uncertainty. Noise filtering works particularly well if the simulation model is a good description of the underlying process or is flexible enough to adapt to the course of the data. In BayModTS, the derived CI tubes are influenced by the choice of the error model, its hyperparameters and the prior. If only limited information about the parameters is known a-priori, non-informative priors can be used. In practice, sampling procedures and optimisation algorithms usually require boundaries, which must be adjusted manually. These bounds should not restrict the sampling, which can be difficult with correlated or sloppy parameters. Model reduction techniques can be used here to improve the identifiability of the simulation model parameters (Eisenkolb *et al.*, 2020).

For future applications, extensions of the workflow are easily possible. First, the method can also be applied to non-time series data. If there is only one dependent variable and serial data with known underlying dynamics, BayModTS can quantify the uncertainty and predict a credible range of the dynamics. To use serial non-time data, the user must define another dependent variable in the SBML file and include the corresponding data in the PEtab measurement table. Second, BayModTS can be applied to user-defined SBML models. This flexibility allows including domain-specific knowledge about the dynamics and interactions of the underlying system. Third, the BayModTS analysis provides SBML models that allow a time-continuous description of experimental data with uncertainty. In the future, these can be used as input modules for other computational models. For example, BayModTS-derived perfusion changes after PVL could be used as input for other liver models, thereby relating liver perfusion to liver function. Fourth, BayModTS can also compare different processes rather than different conditions. Here, different SBML models describing the underlying processes are used for comparison.

Competing interests

No competing interest is declared.

Author contributions statement

SH and NER developed the methodology. SH conducted the Bayesian analyses in close consultation with NER. MK supported FAIR principles. KHH, WTZ, JRR, UD, MA, HMT, and EK collected and curated the data used in this study and helped SH and NER to interpret the BayModTS results in a biomedical context. WW operated the animals of the PVL MRI measurements. All authors wrote and reviewed the manuscript.

Acknowledgments

SH, MA, UD, KHH, MK, JRR, HMT, WTZ and NER were supported by the German Research Foundation (DFG) within the Research Unit Program FOR 5151 "QuaLiPerF (Quantifying Liver Perfusion-Function Relationship in Complex Resection - A Systems Medicine Approach)" by grant number 436883643. SH and NER further acknowledge support by the Deutsche Forschungsgemeinschaft (DFG, German Research Foundation) under Germany's Excellence Strategy - EXC 2075 - 390740016. HMT, EMK, MK and UD were supported by the DFG by grant number 465194077 (Priority Programme SPP 2311, Subproject SimLivA). EMK was supported by the doctoral scholarship "Jena School for Ageing Medicine" (JSAM) of the Else-Kröner-Fresenius Foundation. MA and UD were supported by DFG SteaPKMod grant number 410848700. MK and HMT were supported by the Federal

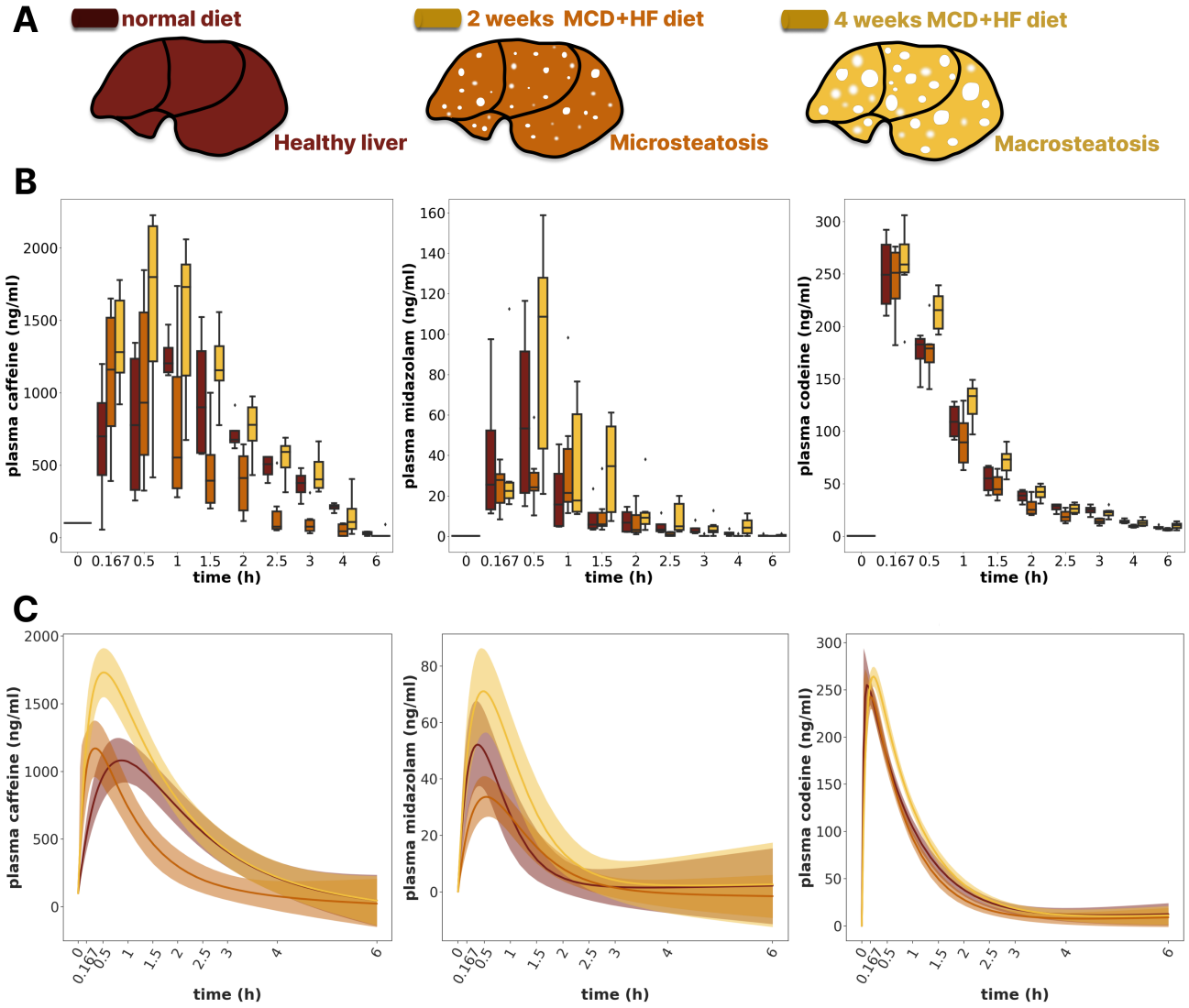

Fig. 4. Effect of severity and pattern of periportal steatosis on pharmacokinetics. A. Mice were fed 2 weeks with normal diet and with Methionine-Choline Deficient (MCD) and High Fat (HF) diet for either 2 or 4 weeks. The MCD+HF diet induces hepatic microsteatos after 2 weeks and macrosteatosis after 4 weeks. B. Boxplots of plasma drug elimination time-courses. The Control group (red) consisted of n=4 animals while the 2 weeks (orange) and 4 weeks (yellow) groups consisted of n=6 animals each. C. Median ensemble prediction (dark lines) and 95% CI tubes of the BayModTS analysis with RTDs.

Ministry of Education and Research (BMBF, Germany) within ATLAS (grant number 031L0304B). WW was supported by the Interdisciplinary Center for Clinical Research (IZKF) of Jena University Hospital (Clinician Scientist Programm CSP 12). We acknowledge the support by the Stuttgart Center for Simulation Science (SimTech). The authors acknowledge support by the High Performance and Cloud Computing Group at the Zentrum für Datenverarbeitung of the University of Tübingen, the state of Baden-Württemberg through bwHPC and the German Research Foundation (DFG) through grant no INST 37/935-1 FUGG. We acknowledge the use of Grammarly for language editing.

References

Abreu, P. *et al.* (2020). Liver resections for metastasis: surgical outcomes of a single center academic institution. *BMC Surgery*, **20**(1), 254.

Albadry, M. *et al.* (2022). Periportal steatosis in mice affects distinct parameters of pericentral drug metabolism. *Scientific Reports*, **12**(1), 21825.

Campagnoli, P. *et al.*, editors (2009). *Dynamic Linear Models with R*. Springer New York, New York, NY.

Chen, C. *et al.* (2022). The area under the effect curve as an efficacy determinant for anti-infectives. *CPT: Pharmacometrics & Systems Pharmacology*, **11**(8), 1029–1044.

Christ, B. *et al.* (2021). Hepatectomy-Induced Alterations in Hepatic Perfusion and Function - Toward Multi-Scale Computational Modeling for a Better Prediction of Post-hepatectomy Liver Function. *Frontiers in Physiology*, **12**.

Eisenkolb, I. *et al.* (2020). Modeling of biocatalytic reactions: A workflow for model calibration, selection, and validation

using bayesian statistics. *AIChE J*, **66**(e16866).

El-Serag, H. B. and Rudolph, K. L. (2007). Hepatocellular carcinoma: epidemiology and molecular carcinogenesis. *Gastroenterology*, **132**(7), 2557–2576.

Elderkin, J. *et al.* (2023). Hepatocellular Carcinoma: Surveillance, Diagnosis, Evaluation and Management. *Cancers*, **15**(21).

Ferlay, J. *et al.* (2015). Cancer incidence and mortality worldwide: sources, methods and major patterns in GLOBOCAN 2012. *International Journal of Cancer*, **136**(5), E359–86.

Foreman-Mackey, D. *et al.* (2013). emcee : The MCMC Hammer. *Publications of the Astronomical Society of the Pacific*, **125**(925), 306–312.

Grubbs, F. E. (1950). Sample Criteria for Testing Outlying Observations. *The Annals of Mathematical Statistics*, **21**(1), 27–58.

Hawkins, D. M. (1980). *Identification of Outliers*. Springer Netherlands, Dordrecht.

Huang, H. *et al.* (2022). Sex-related differences in safety profiles, pharmacokinetics and tissue distribution of sinomenine hydrochloride in rats. *Archives of Toxicology*, **96**(12), 3245–3255.

Hughes, J. H. *et al.* (2019). Optimising time samples for determining area under the curve of pharmacokinetic data using non-compartmental analysis. *The Journal of Pharmacy and Pharmacology*, **71**(11), 1635–1644.

Jahng, G.-H. *et al.* (2014). Perfusion Magnetic Resonance Imaging: A Comprehensive Update on Principles and Techniques. *Korean J Radiol*, **15**(5), 554.

Keating, S. M. *et al.* (2020). SBML Level 3: an extensible format for the exchange and reuse of biological models. *Molecular Systems Biology*, **16**(8), e9110.

Ko, J. *et al.* (2023). Pharmacokinetic Analyses of Liposomal and Non-Liposomal Multivitamin/Mineral Formulations. *Nutrients*, **15**(13).

Korpela, J. *et al.* (2014). Confidence bands for time series data. *Data Mining and Knowledge Discovery*, **28**(5-6), 1530–1553.

Kreutz, C. (2020). A New Approximation Approach for Transient Differential Equation Models. *Frontiers in Physics*, **8**.

Kreutz, C. *et al.* (2007). An error model for protein quantification. *Bioinformatics*, **23**(20), 2747–53.

Kruschke, J. K. (2021). Bayesian Analysis Reporting Guidelines. *Nature Human Behaviour*, **5**(10), 1282–1291.

Reddy, S. K. *et al.* (2011). Major liver resection in elderly patients: a multi-institutional analysis. *J Am Coll Surg*, **212**(5), 787–95.

Rorabacher, D. B. (1991). Statistical treatment for rejection of deviant values: critical values of Dixon's Q parameter and related subrange ratios at the 95% confidence level. *Analytical Chemistry*, **63**(2), 139–146.

Schälte, Y. *et al.* (2021). pyPESTO - Parameter EStimation TOolbox for python.

Scheff, J. D. *et al.* (2011). Assessment of pharmacologic area under the curve when baselines are variable. *Pharmaceutical Research*, **28**(5), 1081–1089.

Schmiester, L. *et al.* (2021). PEtab-Interoperable specification of parameter estimation problems in systems biology. *PLoS Computational Biology*, **17**(1), e1008646.

Tapinos, A. and Mendes, P. (2013). A method for comparing multivariate time series with different dimensions. *PLoS ONE*, **8**(2), e54201.

Thomaseth, C. and Radde, N. (2023). The effect of normalisation and error model choice on the distribution of the maximum likelihood estimator for a biochemical reaction. *IET Syst. Biol.*, **17**(1), 1–13.

Tietjen, G. L. and Moore, R. H. (1972). Some Grubbs-Type Statistics for the Detection of Several Outliers. *Technometrics*, **14**(3), 583–597.

Tiwari, K. *et al.* (2021). Reproducibility in systems biology modelling. *Molecular Systems Biology*, **17**(2), e9982.

Veteläinen, R. *et al.* (2007). Steatosis as a risk factor in liver surgery. *Annals of surgery*, **245**(1), 20–30.

Vogel, A. *et al.* (2018). Hepatocellular carcinoma: ESMO Clinical Practice Guidelines for diagnosis, treatment and follow-up. *Annals of oncology : official journal of the European Society for Medical Oncology*, **29**(Suppl 4), iv238–iv255.

Wei, Y. *et al.* (2022). The Effects of a Novel Curcumin Derivative Loaded Long-Circulating Solid Lipid Nanoparticle on the MHCC-97H Liver Cancer Cells and Pharmacokinetic Behavior. *International Journal of Nanomedicine*, **17**, 2225–2241.

Younossi, Z. M. *et al.* (2023). The global epidemiology of nonalcoholic fatty liver disease (NAFLD) and nonalcoholic steatohepatitis (NASH): a systematic review. *Hepatology (Baltimore, Md.)*, **77**(4), 1335–1347.